IMMUNOLOGY

WDFY4 is required for cross-presentation in response to viral and tumor antigens

Derek J. Theisen[1]*, Jesse T. Davidson IV[1,2]*, Carlos G. Briseño[1], Marco Gargaro[3], Elvin J. Lauron[4], Qiuling Wang[5], Pritesh Desai[1,5], Vivek Durai[1], Prachi Bagadia[1], Joshua R. Brickner[1], Wandy L. Beatty[5], Herbert W. Virgin[1,6], William E. Gillanders[2,7], Nima Mosammaparast[1], Michael S. Diamond[1,5,8,9], L. David Sibley[5], Wayne Yokoyama[4], Robert D. Schreiber[1,9], Theresa L. Murphy[1], Kenneth M. Murphy[1,10]†

During the process of cross-presentation, viral or tumor-derived antigens are presented to CD8$^+$ T cells by *Batf3*-dependent CD8α^+/XCR1$^+$ classical dendritic cells (cDC1s). We designed a functional CRISPR screen for previously unknown regulators of cross-presentation, and identified the BEACH domain–containing protein WDFY4 as essential for cross-presentation of cell-associated antigens by cDC1s in mice. However, WDFY4 was not required for major histocompatibility complex class II presentation, nor for cross-presentation by monocyte-derived dendritic cells. In contrast to *Batf3*$^{-/-}$ mice, *Wdfy4*$^{-/-}$ mice displayed normal lymphoid and nonlymphoid cDC1 populations that produce interleukin-12 and protect against *Toxoplasma gondii* infection. However, similar to *Batf3*$^{-/-}$ mice, *Wdfy4*$^{-/-}$ mice failed to prime virus-specific CD8$^+$ T cells in vivo or induce tumor rejection, revealing a critical role for cross-presentation in antiviral and antitumor immunity.

Presentation of antigens as peptides bound to proteins of the major histocompatibility complex (MHC) is the principal mechanism by which innate cells promote antigen-specific T cell immunity (*1*). Classical dendritic cells (cDCs) are particularly efficient antigen-presenting cells and comprise two major functionally distinct subsets, cDC1 and cDC2 (*2*–*4*). The cDC1 lineage (*2*, *5*) is the most efficient at priming cytotoxic CD8$^+$ T cells to exogenously derived antigens, a process termed cross-presentation (*6*–*10*). This specialization was observed in *Batf3*$^{-/-}$ mice that specifically lack cDC1 development and cannot mount cytotoxic T cell responses to viruses and tumors (*10*–*24*). However, because these studies have only analyzed these responses in the context of mice lacking cDC1s, the role of cross-presentation versus other cDC1-specific effector functions, such as interleukin-12 (IL-12)–mediated protection against *Toxoplasma gondii* (*25*), has remained incompletely understood.

Cross-presentation has been studied using different cell types and various forms of antigen, and not all findings have been confirmed in vivo (*26*). DCs generated from monocytes (moDCs) or whole bone marrow cultured in vitro with granulocyte/macrophage colony-stimulating factor with or without IL-4 (*27*–*29*) are heterogeneous, resembling both macrophages and DCs (*30*), and use a cross-presentation program divergent from that of cDC1s in vivo (*26*, *31*, *32*). Studies of moDCs have produced two major models of cross-presentation: one that involves transport of exogenous antigen to the cytosolic proteasome before peptide loading in the endoplasmic reticulum (ER) (*1*, *7*, *33*–*35*), and another where peptide loading occurs directly in phagosomes by fusion with vesicles containing the peptide-loading complex (*36*, *37*). The latter pathway may be regulated by the SNARE family member Sec22b, although two recent studies of *Sec22b*-deficient mice arrived at different conclusions as to the role of Sec22b in T cell priming to cell-associated antigens in vivo (*38*, *39*). These differences highlight the need for systematic investigation into the mechanisms of cross-presentation in vivo (*39*, *40*).

We established a screen for previously unknown cellular components required for cross-presentation, and optimized in vitro conditions to replicate this process in cDC1s. The efficiency and cell type specificity of cross-presentation can vary, depending on whether the antigen is soluble or associated with cells or pathogens (*32*). Bacterial-associated antigen in the form of heat-killed *Listeria monocytogenes* expressing ovalbumin (HKLM-OVA) was efficiently cross-presented by cDC1s to OT-I T cells but was not presented by cDC2s (Fig. 1A). In contrast, soluble ovalbumin (OVA) was cross-presented by both cDC1 and cDC2 lineages, with lower efficiency in cDC2s by a factor of 3 to 10 (Fig. 1B). Presentation of SIINFEKL (Ser-Ile-Ile-Asn-Phe-Glu-Lys-Leu) peptide to OT-I cells was equally efficient in cDC1s and cDC2s, as expected (Fig. 1C). Previous studies have suggested that the majority of antigens undergo translocation to the cytosol during cross-presentation in vivo (*1*, *7*, *35*). We found that cell-associated antigens, which are presented only by cDC1s and not cDC2s, are *Tap1*-dependent, suggesting presentation through the cytosolic pathway (Fig. 1D). In contrast, soluble antigens were presented by both *Tap1*$^{-/-}$ cDC1s and cDC2s, with only slight differences in efficiency relative to wild-type cDCs (Fig. 1E). For these reasons, we concluded that the use of cell-associated antigens in a screen would best emphasize cDC1-specific processing functions.

Screening could be done using either biochemical detection of peptide:MHC complexes (p:MHCs) or a T cell response. The antibody 25-D1.16 can directly measure SIINFEKL:K^b complexes on the cell surface (*41*); 25-D1.16 detected a robust signal from soluble OVA processed by cDC1s (Fig. 1F), but no signal was detected using an immunogenic dose of cell-associated antigen (Fig. 1G). T cells can respond to only a few hundred p:MHCs (*42*, *43*), implying that the detection limit for 25-D1.16 is greater than that for T cells. Thus, we decided to use T cell proliferation as the readout and determined that 10^4 cDCs can produce a reliable and specific signal of OT-I proliferation (Fig. 1H). We considered gene candidates on the basis of expression in cDCs, relative cDC1 specificity, and gene ontology (table S1). We expressed single guide RNAs (sgRNAs) (*44*) for candidates (table S2) by retrovirus under the U6 promoter and infected DC progenitors from Cas9 transgenic mice (*45*) (fig. S1A). Cells were cultured in Flt3L for 7 days, sorted to purify infected cDCs, and tested for cross-presentation (Fig. 1I and fig. S1, B and C).

Cross-presentation was substantially impaired by two independent sgRNAs for *Wdfy4* (WD repeat- and FYVE domain–containing protein 4), a member of the BEACH (Beige and Chediak-Higashi) domain–containing family of proteins (*46*) (Fig. 2A and fig. S1C). *Wdfy4* is highly expressed in mouse and human cDC1s (fig. S2), with 80% species similarity (*47*). WDFY4 is one of nine BEACH domain–containing proteins (BDCPs) (*46*) and has three closely related family members. However, CRISPR targeting using sgRNAs for *Wdfy1*, *Wdfy2*, and *Wdfy3* did not impair cross-presentation, in contrast to *Wdfy4* (Fig. 2B). Thus, *Wdfy4* appears to be unique within this gene family for supporting cross-presentation by cDC1s.

[1]Department of Pathology and Immunology, Washington University School of Medicine, St. Louis, MO 63110, USA. [2]Department of Surgery, Washington University School of Medicine, St. Louis, MO 63110, USA. [3]Department of Experimental Medicine, University of Perugia, Perugia, Italy. [4]Division of Rheumatology, Department of Medicine, Washington University School of Medicine, St. Louis, MO 63110, USA. [5]Department of Molecular Microbiology, Washington University School of Medicine, St. Louis, MO 63110, USA. [6]Vir Biotechnology, San Francisco, CA, USA. [7]Alvin J. Siteman Cancer Center at Barnes-Jewish Hospital and Washington University School of Medicine, St. Louis, MO 63110, USA. [8]Department of Medicine, Washington University School of Medicine, St. Louis, MO 63110, USA. [9]Andrew M. and Jane M. Bursky Center for Human Immunology and Immunotherapy Programs, Washington University School of Medicine, St. Louis, MO 63110, USA. [10]Howard Hughes Medical Institute, Washington University School of Medicine, St. Louis, MO 63110, USA.
*These authors contributed equally to this work.
†Corresponding author. Email: kmurphy@wustl.edu

To evaluate the in vivo function of *Wdfy4*, we obtained mice with exon 4 deleted by CRISPR/Cas9 genome editing, leading to translational termination due to a reading frame shift when exon 3 splices to exon 5 (fig. S3). *Wdfy4*$^{-/-}$ mice were viable, born in normal Mendelian ratios, and displayed normal development of hematopoietic lineages, including cDCs (Fig. 2, C and D, and fig. S4), which expressed *Irf8* and had normal turnover kinetics (fig. S4, H and I), and T cells (fig. S5). In particular, cDC1s developed in *Wdfy4*$^{-/-}$ mice, unlike *Batf3*$^{-/-}$ mice, and expressed CD24, XCR1, and CD103 normally (Fig. 2, C and D, and fig. S4, B and F). However, cDC1s from *Wdfy4*$^{-/-}$ mice showed a striking defect in cross-presentation of both cell-associated and bacterial-associated antigen in vitro (Fig. 2, E and F, and fig. S6A) and showed reduced efficiency for soluble OVA presentation relative to wild-type cDC1s (Fig. 2G). Notably, *Wdfy4*$^{-/-}$ cDC1s cross-presented soluble OVA with the efficiency of cDC2s, which were not influenced by the loss of *Wdfy4* (Fig. 2G). However, *Wdfy4*$^{-/-}$ cDC1s could directly present antigen introduced into the cytoplasm by osmotic shock or virus, a process that is equally efficient in cDC1s and cDC2s (fig. S6, B to D); this finding suggests that *Wdfy4*$^{-/-}$ cDC1s have the capacity to present endogenous antigens on MHC class I complexes.

moDCs can cross-present both soluble and cell-associated antigens in vitro (*27*, *48*, *49*), but their transcriptional program is distinct from that of cDC1 (*31*). We found that moDCs derived from wild-type and *Wdfy4*$^{-/-}$ mice cross-present antigens with the same efficiency, both for cell-associated (fig. S6E) and soluble OVA (fig. S6F), which suggests that moDCs use a *Wdfy4*-independent pathway for cross-presentation. The defect in cross-presentation by *Wdfy4*$^{-/-}$ cDC1s is specific, because MHC class II antigen processing was unchanged in *Wdfy4*$^{-/-}$ mice for both cell-associated and soluble antigens (Fig. 2H and fig. S6G). MHC class II antigen processing by B cells was also normal in *Wdfy4*$^{-/-}$ mice (fig. S7A), which were able to generate germinal center B cells and T follicular helper (T_{FH}) cells in response to immunization with sheep red blood cells (fig. S7, B to E).

cDCs from *Wdfy4*$^{-/-}$ mice expressed normal levels of MHC class I at steady state and after activation (fig. S8, A and B), up-regulated the costimulatory molecules CD80/86, and expressed cytokines normally (fig. S8, C to F). Loss of *Wdfy4* also did not influence gene expression in cDC1s at steady state or after activation in tumor-bearing mice (fig. S8, G and H). Despite their inability to cross-present, *Wdfy4*$^{-/-}$ cDC1s were capable of taking up and degrading soluble antigens normally (fig. S9, A and B) and phagocytosing labeled HKLM-OVA, as seen both microscopically (fig. S9C) and by quantification of this phagocytosis as measured by fluorescence-activated cell sorting (FACS) (fig. S9D).

To explore the mechanism of action of WDFY4, we analyzed various cellular compartments of wild-type and *Wdfy4*$^{-/-}$ cDC1s by confocal microscopy and found minimal differences in distribution of MHC class I stores, ER, early endosomes, lysosomes, late endosomes, or the peptide-loading complex at steady state (fig. S10). In addition, we observed minimal differences in distribution of Rab43 [a molecule previously described to be involved in cross-presentation (*32*)], p62 (autophagic vesicles), Rab7 (late endosomes), or Lamp1 (lysosomes) after antigen phagocytosis (fig. S11). Electron microscopy of WDFY4-deficient ex vivo cDC1s showed the presence of large and numerous lipid bodies throughout the cytoplasm that were not present in wild-type cells (figs. S12 and S13, A and C). However, these lipid bodies were not present in Flt3L-derived cDC1s from *Wdfy4*$^{-/-}$ mice (fig. S13, B and C), which still had a defect in cross-presentation of cell-associated antigen (fig. S13D); this finding suggests that the lipid bodies are not necessary to cause the defect in cross-presentation in *Wdfy4*$^{-/-}$ cDC1s.

To determine the interacting partners of WDFY4, we generated four individually FLAG-tagged subregions of WDFY4 spanning the entire protein (Fig. 3A). We stably transduced these fragments into the murine DC line JAWSII (*50*) and performed affinity purification mass spectrometry (AP-MS) to isolate WDFY4 binding partners. We found 143 candidates enriched by different regions of the WDFY4 protein, with the largest number binding to the FL4 fragment of WDFY4 that contains the pleckstrin homology (PH), BEACH, WD40, and FYVE domains (Fig. 3A and table S3). We performed gene ontology analysis

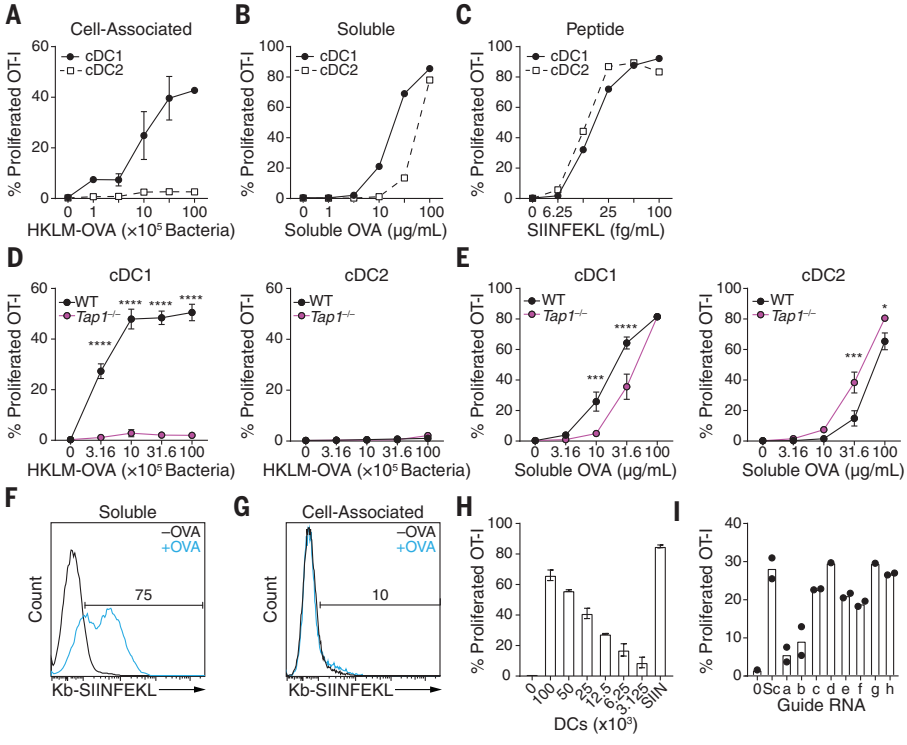

Fig. 1. Establishment of a CRISPR/Cas9 screen for cross-presentation of cell-associated antigens. (**A** to **C**) Sort-purified cDC1s and cDC2s were cultured for 3 days with increasing concentrations of HKLM-OVA (A), soluble OVA (B), or SIINFEKL peptide (C) and CFSE-labeled OT-I T cells and assayed for proliferation (CFSE^{-}CD44^{+}). (**D** and **E**) Wild-type (WT) or *Tap1*$^{-/-}$ sort-purified cDC1s and cDC2s were cultured for 3 days with varying concentrations of HKLM-OVA (D) or soluble OVA (E) and CFSE-labeled OT-I T cells and assayed for proliferation (CFSE^{-}CD44^{+}). (**F** and **G**) Sorted cDC1s were cultured with soluble OVA (100 μg/ml) (F) or 10^6 splenocytes osmotically loaded with OVA (G) for 48 hours, stained with 25-D1.16, and analyzed by flow cytometry. (**H**) CFSE-labeled OT-I cells were cultured with the indicated number of whole Flt3L-generated DCs and either 10^7 HKLM-OVA or SIINFEKL peptide (SIIN; 25 fg/ml), and proliferation was measured as in (A). (**I**) c-Kit^{hi} bone marrow progenitors from Cas9 transgenic mice were infected with retroviruses expressing various sgRNAs (table S2) and cultured with Flt3L for 7 days, and infected cDCs were tested for cross-presentation to CFSE-labeled OT-I T cells as in (H). Sc, scramble; activated T cells were gated as CFSE^{-}CD44^{+}. Data are means ± SEM. *P < 0.05, ***P < 0.001, ****P < 0.0001 [two-way analysis of variance (ANOVA) with Tukey multiple-comparisons test].

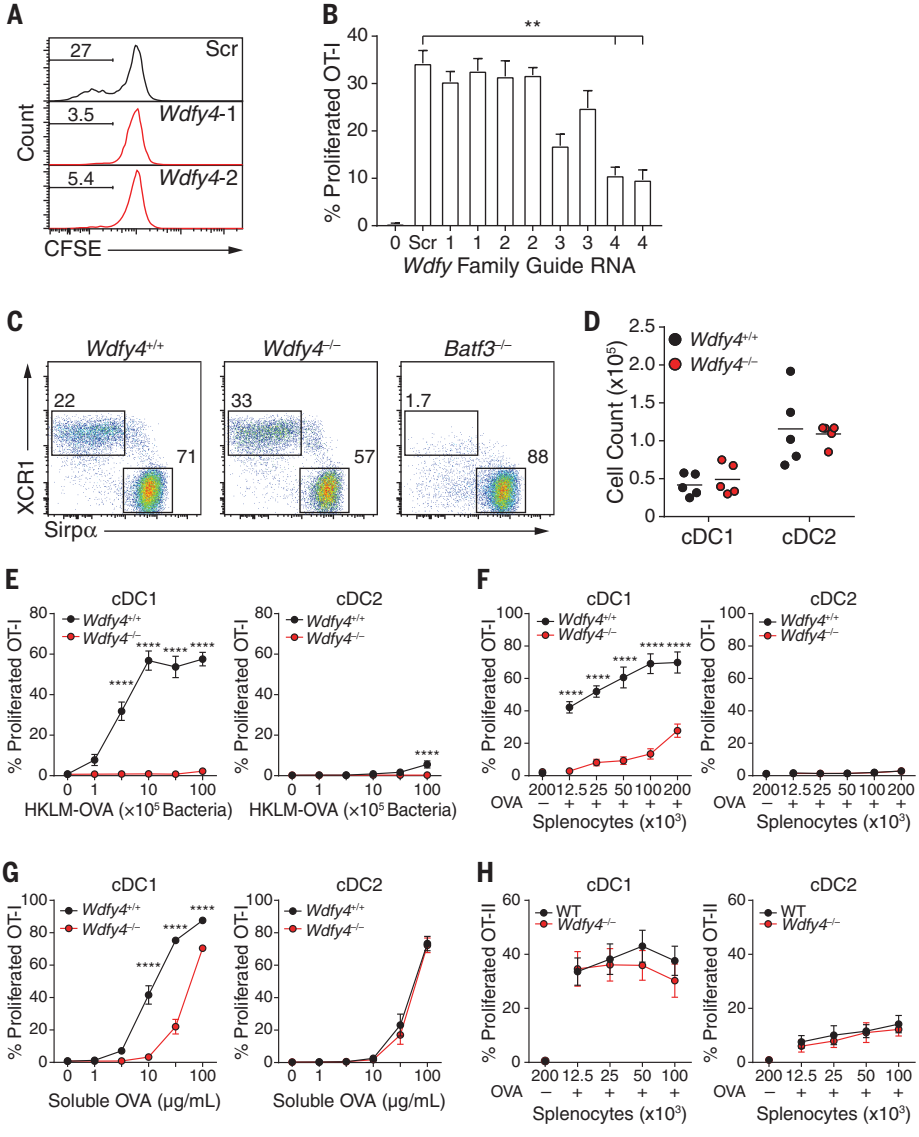

Fig. 2. *Wdfy4* is selectively required for cross-presentation of cell-associated antigens by cDC1s. (**A**) Cross-presentation was measured for Cas9-transgenic cDC1s expressing two sgRNAs (1 and 2; middle and bottom) for *Wdfy4* or a scramble control (Scr; top) that were generated as described in Fig. 1I. T cell proliferation is shown by percentages of $CFSE^-$ OT-I cells. (**B**) Cross-presentation by cDC1s expressing sgRNAs for *Wdfy1*, *Wdfy2*, *Wdfy3*, and *Wdfy4* was measured as described in Fig. 1I. Activated T cells were gated as $CFSE^-CD44^+$. Data are means ± SEM of three independent experiments. (**C**) cDC1 and cDC2 development was assessed by flow cytometry in wild-type, $Wdfy4^{-/-}$, and $Batf3^{-/-}$ mice; plots were pre-gated as $B220^-CD11c^+MHCII^+$ and then gated as cDC1 ($XCR1^+Sirp\alpha^-$) or cDC2 ($XCR1^-Sirp\alpha^+$). (**D**) Absolute cell numbers of cDC1s and cDC2s in wild-type and $Wdfy4^{-/-}$ mice. Each dot indicates one mouse; bar indicates mean. (**E**) FACS-sorted cDC1s and cDC2s from spleens of wild-type and $Wdfy4^{-/-}$ mice were assayed for presentation to OT-I ($CFSE^-CD44^+$) in response to the indicated concentrations of HKLM-OVA. (**F**) FACS-sorted cDC1s and cDC2s from spleens of bone marrow chimeric mice with wild-type or $Wdfy4^{-/-}$ bone marrow were assayed for presentation to OT-I ($CFSE^-CD44^+$) in response to the indicated concentrations of OVA-loaded irradiated splenocytes from MHC class I triple knockout ($K^{b-/-}$, $K^{d-/-}$, $\beta2m^{-/-}$) mice. (**G**) FACS-sorted cDC1s and cDC2s from spleens of wild-type and $Wdfy4^{-/-}$ mice were assayed for presentation to OT-I ($CFSE^-CD44^+$) in response to the indicated concentrations of soluble OVA. (**H**) FACS-sorted cDC1s and cDC2s from spleens of wild-type and $Wdfy4^{-/-}$ mice were assayed for presentation to OT-II ($CFSE^-CD44^+$) in response to the indicated concentrations of OVA-loaded irradiated splenocytes from MHC class II knockout mice. In (F) and (H), OVA– denotes a negative control of splenocytes osmotically pulsed in the absence of OVA. Data are means ± SEM from three independent experiments. *$P < 0.05$, **$P < 0.01$, ****$P < 0.0001$ (two-way ANOVA with Tukey multiple-comparisons test).

to determine the biological processes most likely influenced by WDFY4 (*51*). The fragments FL1 and FL2 of WDFY4 associated with proteins involved in "protein complex assembly," and therefore they may be involved in forming multimeric protein structures or scaffolding vesicular machinery (Fig. 3B and table S4). FL3 and FL4 associated with proteins involved in "protein localization," "vesicle transport," and "cytoskeletal organization," suggesting a role for WDFY4 in proper subcellular vesicular targeting (Fig. 3C and table S5). Notably, FL4 associated with components critical to the formation, function, and trafficking of endocytic vesicles, including clathrin (*Cltc*, *Clta*) (*52*), subunits of the AP-2 clathrin adaptor complex (*Ap2a1*, *Ap2a2*, *Ap2b1*) (*52*), modulators of cytoskeleton dynamics (*Iqgap1*, *Actn4*) (*53*, *54*), and several members of the vacuolar-type (H^+) adenosine triphosphatase complex (*Atp6v0a3*, *Atp6va1*, *Atp6v1f*) (*55*) (Fig. 3D and tables S3 and S6). FL4 also selectively associated with *Hsp90ab1*, a member of the HSP90 chaperone family involved in endosome-to-cytosol translocation of antigen during cross-presentation (*56*–*59*) (Fig. 3, D to F). Although heat shock proteins such as *Hspa8* and *Hsp1a1* can appear as artifacts in AP-MS data because of their function as chaperones (*60*), *Hsp90ab1* is rarely detected in this manner, and therefore its association may represent a functional interaction with WDFY4.

We then sought to determine which vesicles WDFY4 may be acting on by determining its intracellular location. We visualized full-length Twin-Strep-tagged (*61*) WDFY4 in JAWSII cells by confocal microscopy and found that it localized to the periphery of the cytosol near the plasma membrane (Fig. 3G). WDFY4 was poorly colocalized with the cell surface receptor DEC-205, intracellular MHC class I stores, and lysosomes, but demonstrated moderate colocalization with early endosomes and the ER. cDC1s were previously shown to have well-defined and extensive ER structures that may extend throughout the cytosol near vesicular compartments (*62*) and may lead to colocalization with components of the endosomal pathway. WDFY4 showed the highest correlation with the endosomal markers clathrin and Rab11 (Fig. 3, G and H), which suggests that it localizes to an endosomal compartment near the plasma membrane. Taken together, these data suggest that WDFY4 functions in trafficking between the cell surface and endosomes, and thus may regulate multimeric protein assembly required for the proper formation and localization of endocytic vesicles.

We then examined the role of WDFY4 in cross-presentation of cell-associated antigens in vivo. Carboxyfluorescein succinimidyl ester (CFSE)–labeled OT-I T cells showed strong in vivo proliferation induced by immunization with OVA-loaded splenocytes when transferred into $Wdfy4^{+/-}$ mice, but not when transferred into $Wdfy4^{-/-}$ mice (Fig. 4, A and B), confirming an in vivo defect in cross-presentation. IL-12 produced by cDC1s in response to soluble tachyzoite antigen (STAg) is required for innate immune protection against

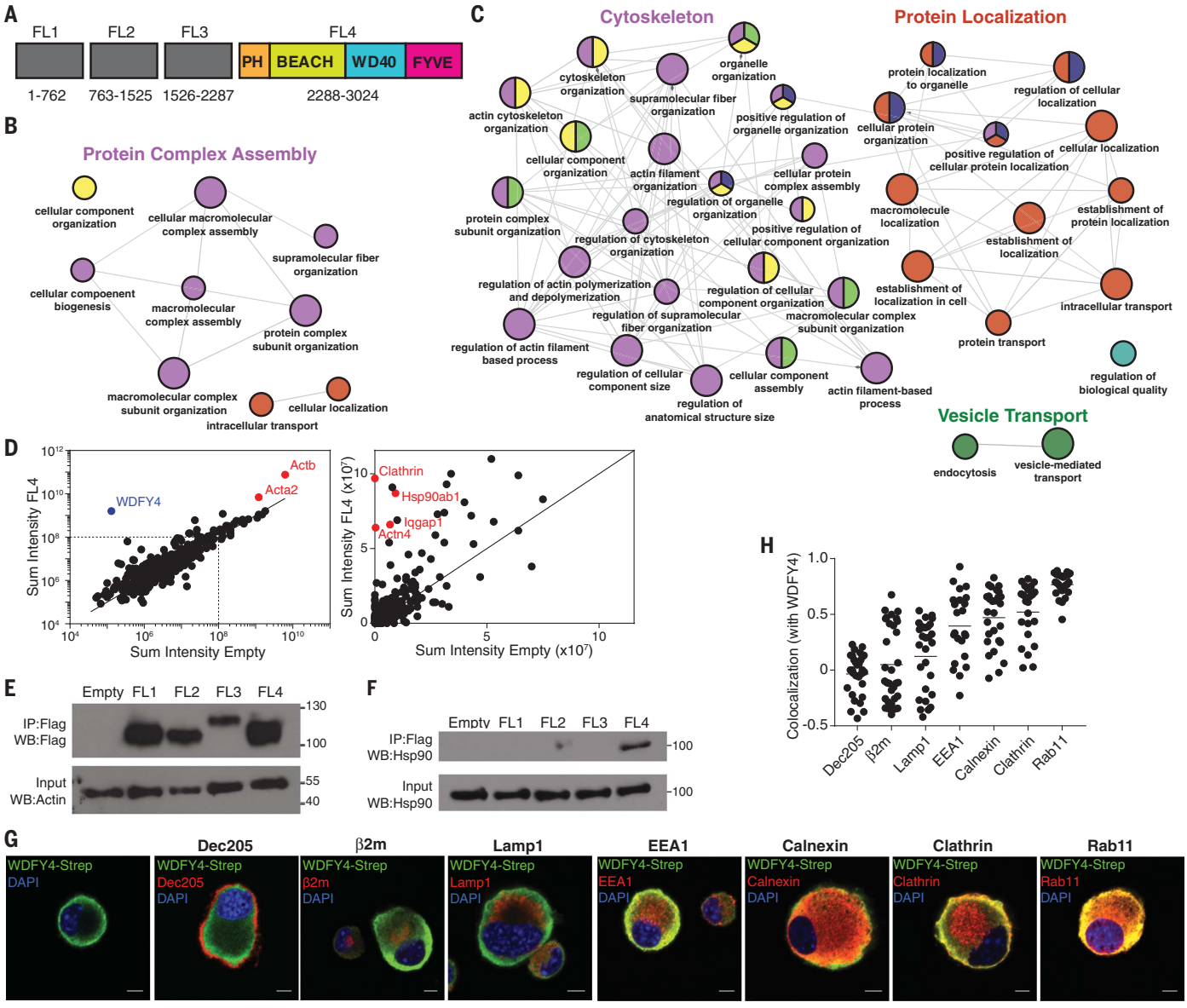

Fig. 3. WDFY4 acts near the plasma membrane and associates with proteins involved in localization and vesicular transport. (**A**) Diagram of truncated fragments of WDFY4 protein, showing predicted domains within the FL4 fragment. Numbers indicate amino acid locations of fragments. (**B**) ClueGO visualization of gene ontology terms enriched after immunoprecipitation of fragments from (A) in the mouse DC line JAWSII, expressing either FL1 or FL2 fragments. Small circles, $P < 0.001$; large circles, $P < 0.0001$. Colors indicate gene ontology (GO) term groups. (**C**) ClueGO visualization of gene ontology terms enriched after immunoprecipitation of fragments from (A) in the mouse DC line JAWSII expressing either FL3 or FL4 fragments. Small circles, $P < 3 \times 10^{-5}$; large circles, $P < 3 \times 10^{-6}$. Colors indicate GO term groups. (**D**) Scatterplot of representative data for sum intensity of proteins found after mass spectrometry between FL4-expressing and empty vector–expressing JAWSII cells. (**E**) Western blot of Flag immunoprecipitates from human embryonic kidney (HEK) 293 cells transfected with empty vector or Flag-tagged WDFY4 fragments 1 to 4 (top) and input control for β-actin (bottom) (**F**) Western blot for endogenous Hsp90 in Flag immunoprecipitates from HEK293 transfected with empty vector or Flag-tagged WDFY4 fragments 1 to 4 (top) and input control for endogenous Hsp90 (bottom). (**G**) Confocal microscopy of JAWSII cells overexpressing full-length Twin-Strep-tagged WDFY4, stained for anti-Strep (green), various cellular markers (red), and 4′,6-diamidino-2-phenylindole (DAPI; blue). Scale bars, 5 μm. (**H**) Quantification of colocalization between WDFY4 and intracellular markers from images in (G). Each dot represents one cell; bar indicates the mean.

T. gondii, as illustrated by the susceptibility of *Batf3*$^{-/-}$ mice to lethal infection by this pathogen (*25*). In contrast, *Wdfy4*$^{-/-}$ mice were resistant to *T. gondii* infection, similar to *Wdfy4*$^{+/-}$ mice (Fig. 4C). These results indicate that cross-presentation is not required for innate protection against *T. gondii* and that *Wdfy4*$^{-/-}$ cDC1s are not globally impaired in function.

We also evaluated CD8^{+} T cell responses of *Wdfy4*$^{-/-}$ mice to cowpox virus infection, a model in which effective CD8^{+} T cell priming is thought to be mediated primarily by *Batf3*-dependent cells through cross-presentation (*13*). *Batf3*$^{-/-}$ mice that lack cDC1s (*10*–*13*) have a defect in priming antigen-specific CD8^{+} T cells to several viruses (*10*–*13*), but these studies only indirectly show that this is due to a lack of cross-presentation, as loss of alternative functions of cDC1s could conceivably be the cause. However, we found that *Wdfy4*$^{-/-}$ mice that retain cDC1 cells that are unable to cross-present also have severely impaired antigen-specific CD8^{+} T cell responses to cowpox virus (Fig. 4, D and E, and fig. S14, A to D). This defect in cross-presentation

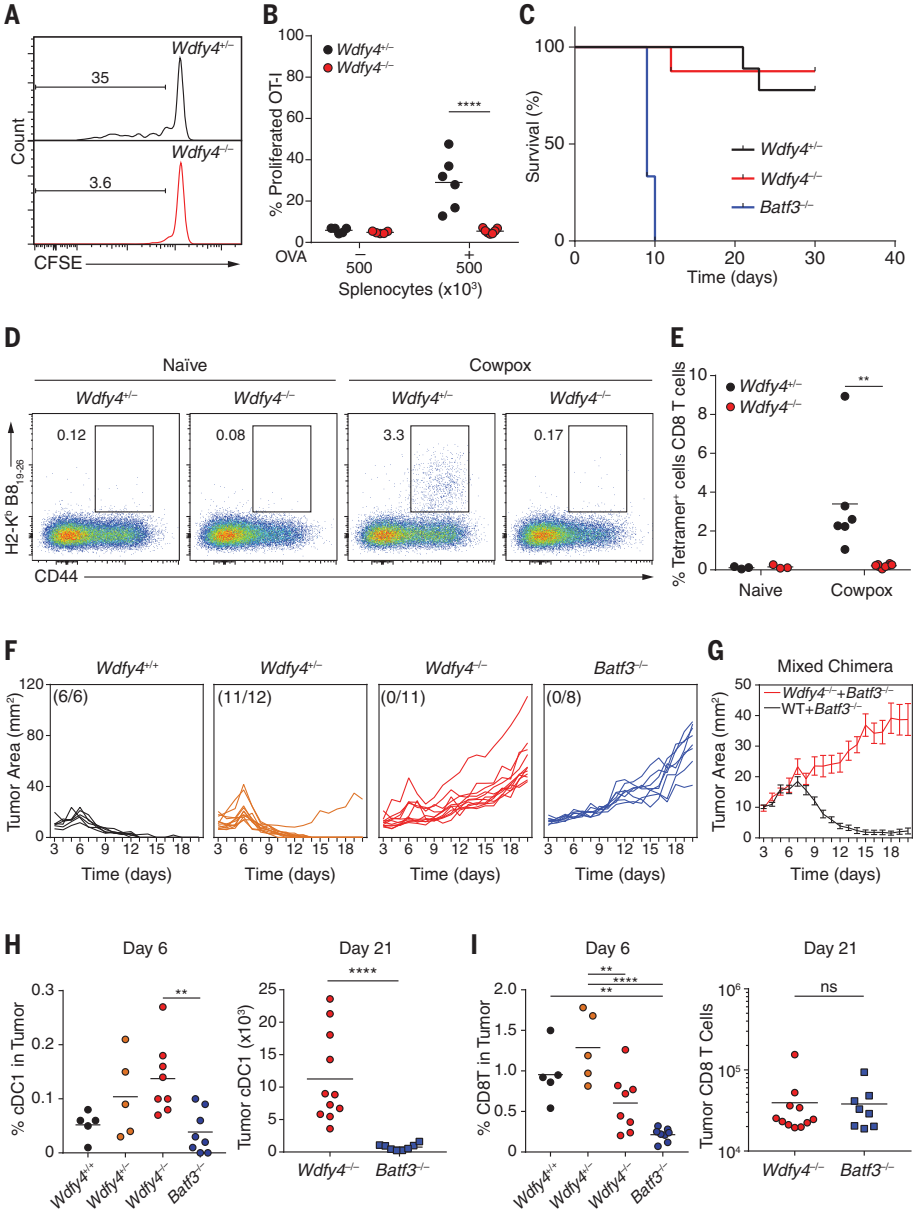

Fig. 4. *Wdfy4*$^{-/-}$ mice are unable to cross-present in vivo. (**A** and **B**) Representative flow cytometry analysis of in vivo cross-presentation to 500,000 irradiated splenocytes loaded with OVA injected intravenously into mice of the indicated genotypes 1 day after injection of 500,000 CFSE-labeled OT-I cells. Mice were harvested 3 days after antigen injection, quantified in (B). Data are pre-gated on OT-I cells and are shown as percentage of CFSE^{-} cells (A) or CFSE^{-}CD44^{+} cells (B). Data are pooled from three independent experiments; each point represents one mouse. (**C**) Survival of mice of the indicated genotypes to injection of 200 Pru.luc *T. gondii* tachyzoites over 30 days. *Wdfy4*$^{+/-}$, $n = 9$; *Wdfy4*$^{-/-}$, $n = 8$; *Batf3*$^{-/-}$, $n = 3$. (**D** and **E**) Representative flow cytometry plots of CD8 T cells (pre-gated CD4^{-}CD3^{+}CD8^{+}) in lungs of naïve or cowpox-infected mice, quantified in (E). Each dot represents one mouse; bar indicates mean. (**F**) Mice of the indicated genotypes were injected with 10^6 fibrosarcoma cells subcutaneously (s.c.) and tumors were measured daily starting at day 3 after injection. (**G**) Mixed bone marrow chimeras with bone marrow of the indicated genotypes were injected into lethally irradiated CD45.1^{+} wild-type B6 mice. Eight weeks later, mice were injected with 10^6 fibrosarcoma cells s.c. and tumors were measured daily starting at day 3 after injection. Data are means ± SEM of nine mice per group. (**H**) Quantification of cDC1s in tumors at either day 6 or day 21 after injection taken from mice of the indicated genotypes. cDC1s were gated as B220^{-}CD11c^{+}MHCII^{+}CD103^{+}CD11b^{-}. Each dot indicates one mouse; bar indicates mean. (**I**) Quantification of CD8 T cells in tumors at either day 6 or day 21 after injection taken from mice of the indicated genotypes. CD8^{+} T cells were gated as CD45^{+}TCRβ^{+}CD8α^{+}CD4^{-}. Each dot indicates one mouse; bar indicates mean. $^{**}P < 0.01$, $^{****}P < 0.0001$ (two-way ANOVA with Tukey multiple-comparisons test); ns, not significant.

is not restricted to cowpox virus, because *Wdfy4*$^{-/-}$ mice also showed a defect in priming CD8^{+} T cells to infection by West Nile virus (fig. S14E). Furthermore, *Wdfy4*$^{-/-}$ mice showed normal priming of CD4^{+} T cells to West Nile, indicating that WDFY4 functions for in vivo cross-presentation to CD8^{+} T cells, but not for priming of CD4^{+} T cells (fig. S14F).

Studies with *Batf3*$^{-/-}$ mice suggested that cDC1s were required for tumor rejection (*10*). To examine the role of cross-presentation directly, we evaluated the growth of the highly immunogenic 1969 regressor fibrosarcoma (*15*) in wild-type, *Wdfy4*$^{+/-}$, *Wdfy4*$^{-/-}$, and *Batf3*$^{-/-}$ mice (Fig. 4F). Tumors were readily rejected by wild-type mice but not by *Batf3*$^{-/-}$ mice (Fig. 4F), as expected (*15*). However, tumors were also rejected by heterozygous *Wdfy4*$^{+/-}$ mice but grew uncontrolled in *Wdfy4*$^{-/-}$ mice, similar to *Batf3*$^{-/-}$ mice (Fig. 4F and fig. S15A). These results with germline-deficient *Wdfy4*$^{-/-}$ mice indicate an in vivo requirement for WDFY4 in tumor rejection but do not pinpoint its function to cDC1s. To test whether the in vivo defect in *Wdfy4*$^{-/-}$ mice is cDC1-intrinsic, we generated mixed bone marrow chimeras using mixtures of either wild-type:*Batf3*$^{-/-}$ or *Wdfy4*$^{-/-}$:*Batf3*$^{-/-}$ bone marrow (Fig. 4G). Wild-type:*Batf3*$^{-/-}$ chimeras rejected tumors normally, but *Wdfy4*$^{-/-}$:*Batf3*$^{-/-}$ chimeras, in which cDC1s develop only from the *Wdfy4*$^{-/-}$ bone marrow, failed to control tumor growth (Fig. 4G). These results indicate that the defect in tumor rejection results from loss of Wdfy4 expression in cDC1s. Notably, in *Wdfy4*$^{-/-}$ mice, cDC1s did infiltrate into tumors as they expanded (Fig. 4H and fig. S15B), yet they induced less recruitment of CD8^{+} T cells to tumors, similar to the lack of CD8^{+} T cells in tumors in *Batf3*$^{-/-}$ mice (Fig. 4I).

WDFY4 is one of nine mammalian BDCPs that typically also contain a PH-like domain and WD repeats (*46*). BDCPs function as protein scaffolds that regulate intracellular vesicle fission and fusion events, and several are associated with human diseases (*46*). For example, mutations in *Lyst* cause Chédiak-Higashi syndrome, a primary immunodeficiency disorder characterized by defective neutrophil phagolysosome formation and cytotoxic T cell degranulation (*63*, *64*). Mutations in *Lrba* result in immune dysregulation in regulatory T cells due to improper trafficking of CTLA4 from endosomes to lysosomes by the clathrin adaptor AP-1 (*65*, *66*). WDFY3, the closest WDFY4 homolog, regulates recruitment of polyubiquitinated protein aggregates to autophagosomes by

interactions with p62, Atg5, Atg12, Atg16L, LC3, and TRAF6 (*67*–*70*). Although cross-presentation of cell-associated antigens does not involve autophagy (*71*), WDFY4 conceivably may regulate vesicular trafficking pathways, a concept supported by its localization to submembrane endosomes and its interaction with endocytic and cytoskeletal machinery. These WDFY4-dependent trafficking pathways may be required for translocation of dead-cell antigen ligated by the cDC1-specific receptor CLEC9A (*72*) to specific compartments to promote cross-presentation (*73*). Further investigation of the mechanisms of WDFY4 may elucidate previously unknown components of the cross-presentation pathway and thus offer therapeutic targets for human disease.

REFERENCES AND NOTES

1. J. S. Blum, P. A. Wearsch, P. Cresswell, *Annu. Rev. Immunol.* **31**, 443–473 (2013).
2. T. L. Murphy *et al*., *Annu. Rev. Immunol.* **34**, 93–119 (2016).
3. V. Durai, K. M. Murphy, *Immunity* **45**, 719–736 (2016).
4. M. Guilliams *et al*., *Nat. Rev. Immunol.* **14**, 571–578 (2014).
5. K. Crozat *et al*., *J. Immunol.* **187**, 4411–4415 (2011).
6. M. J. Bevan, *J. Exp. Med.* **143**, 1283–1288 (1976).
7. O. P. Joffre, E. Segura, A. Savina, S. Amigorena, *Nat. Rev. Immunol.* **12**, 557–569 (2012).
8. J. M. den Haan, S. M. Lehar, M. J. Bevan, *J. Exp. Med.* **192**, 1685–1696 (2000).
9. D. Dudziak *et al*., *Science* **315**, 107–111 (2007).
10. K. Hildner *et al*., *Science* **322**, 1097–1100 (2008).
11. N. Torti, S. M. Walton, K. M. Murphy, A. Oxenius, *Eur. J. Immunol.* **41**, 2612–2618 (2011).
12. K. Nopora *et al*., *Front. Immunol.* **3**, 348 (2012).
13. M. D. Gainey, J. G. Rivenbark, H. Cho, L. Yang, W. M. Yokoyama, *Proc. Natl. Acad. Sci. U.S.A.* **109**, E3260–E3267 (2012).
14. M. B. Fuertes *et al*., *J. Exp. Med.* **208**, 2005–2016 (2011).
15. M. S. Diamond *et al*., *J. Exp. Med.* **208**, 1989–2003 (2011).
16. T. Toubai *et al*., *Blood* **121**, 4231–4241 (2013).
17. X. Yu *et al*., *Cancer Res.* **73**, 2093–2103 (2013).
18. O. A. Ali *et al*., *Cancer Res.* **74**, 1670–1681 (2014).
19. Y. Zhang *et al*., *J. Immunol.* **194**, 5937–5947 (2015).
20. A. Tzeng *et al*., *Cell Rep.* **17**, 2503–2511 (2016).
21. A. R. Sánchez-Paulete *et al*., *Cancer Discov.* **6**, 71–79 (2016).
22. K. D. Moynihan *et al*., *Nat. Med.* **22**, 1402–1410 (2016).
23. B. H. Kwan *et al*., *J. Exp. Med.* **214**, 1679–1690 (2017).
24. S. Spranger, D. Dai, B. Horton, T. F. Gajewski, *Cancer Cell* **31**, 711–723.e4 (2017).
25. M. Mashayekhi *et al*., *Immunity* **35**, 249–259 (2011).
26. D. Theisen, K. Murphy, *F1000 Res.* **6**, 98 (2017).
27. F. Sallusto, A. Lanzavecchia, *J. Exp. Med.* **179**, 1109–1118 (1994).
28. C. Caux, C. Dezutter-Dambuyant, D. Schmitt, J. Banchereau, *Nature* **360**, 258–261 (1992).
29. K. Inaba *et al*., *J. Exp. Med.* **176**, 1693–1702 (1992).
30. J. Helft *et al*., *Immunity* **42**, 1197–1211 (2015).
31. C. G. Briseño *et al*., *Cell Rep.* **15**, 2462–2474 (2016).
32. N. M. Kretzer *et al*., *J. Exp. Med.* **213**, 2871–2883 (2016).
33. M. Kovacsovics-Bankowski, K. L. Rock, *Science* **267**, 243–246 (1995).
34. V. G. Morón, P. Rueda, C. Sedlik, C. Leclerc, *J. Immunol.* **171**, 2242–2250 (2003).
35. F. M. Cruz, J. D. Colbert, E. Merino, B. A. Kriegsman, K. L. Rock, *Annu. Rev. Immunol.* **35**, 149–176 (2017).
36. J. D. Pfeifer *et al*., *Nature* **361**, 359–362 (1993).
37. L. Shen, L. J. Sigal, M. Boes, K. L. Rock, *Immunity* **21**, 155–165 (2004).
38. I. Cebrian *et al*., *Cell* **147**, 1355–1368 (2011).
39. A. Alloatti *et al*., *J. Exp. Med.* **214**, 2231–2241 (2017).
40. S. J. Wu *et al*., *Cell Rep.* **19**, 2645–2656 (2017).
41. A. Porgador, J. W. Yewdell, Y. Deng, J. R. Bennink, R. N. Germain, *Immunity* **6**, 715–726 (1997).
42. C. V. Harding, E. R. Unanue, *Nature* **346**, 574–576 (1990).
43. E. R. Christinck, M. A. Luscher, B. H. Barber, D. B. Williams, *Nature* **352**, 67–70 (1991).
44. L. Cong *et al*., *Science* **339**, 819–823 (2013).
45. R. J. Platt *et al*., *Cell* **159**, 440–455 (2014).
46. A. R. Cullinane, A. A. Schäffer, M. Huizing, *Traffic* **14**, 749–766 (2013).
47. UniProt Consortium, *Nucleic Acids Res.* **45**, D158–D169 (2017).
48. P. Schnorrer *et al*., *Proc. Natl. Acad. Sci. U.S.A.* **103**, 10729–10734 (2006).
49. E. Segura, A. L. Albiston, I. P. Wicks, S. Y. Chai, J. A. Villadangos, *Proc. Natl. Acad. Sci. U.S.A.* **106**, 20377–20381 (2009).
50. V. McKay, E. E. Moore, U.S. Patent 5,648,219 (1997).
51. G. Bindea *et al*., *Bioinformatics* **25**, 1091–1093 (2009).
52. M. Kaksonen, A. Roux, *Nat. Rev. Mol. Cell Biol.* **19**, 313–326 (2018).
53. A. C. Hedman, J. M. Smith, D. B. Sacks, *EMBO Rep.* **16**, 427–446 (2015).
54. D. G. Thomas, D. N. Robinson, *Semin. Cell Dev. Biol.* **71**, 68–74 (2017).
55. K. C. Jefferies, D. J. Cipriano, M. Forgac, *Arch. Biochem. Biophys.* **476**, 33–42 (2008).
56. H. Zheng, Z. Li, *J. Immunol.* **173**, 5929–5933 (2004).
57. T. Ichiyanagi *et al*., *J. Immunol.* **185**, 2693–2700 (2010).
58. T. Imai *et al*., *Proc. Natl. Acad. Sci. U.S.A.* **108**, 16363–16368 (2011).
59. Y. Kato *et al*., *Autoimmune Dis.* **2012**, 745962 (2012).
60. D. Mellacheruvu *et al*., *Nat. Methods* **10**, 730–736 (2013).
61. M. R. Junttila, S. Saarinen, T. Schmidt, J. Kast, J. Westermarck, *Proteomics* **5**, 1199–1203 (2005).
62. F. Osorio *et al*., *Nat. Immunol.* **15**, 248–257 (2014).
63. C. M. Perou *et al*., *Nat. Genet.* **13**, 303–308 (1996).
64. D. L. Nagle *et al*., *Nat. Genet.* **14**, 307–311 (1996).
65. B. Lo *et al*., *Science* **349**, 436–440 (2015).
66. B. Lo *et al*., *Blood* **128**, 1037–1042 (2016).
67. A. Simonsen *et al*., *J. Cell Sci.* **117**, 4239–4251 (2004).
68. T. H. Clausen *et al*., *Autophagy* **6**, 330–344 (2010).
69. M. Filimonenko *et al*., *Mol. Cell* **38**, 265–279 (2010).
70. P. Isakson *et al*., *Autophagy* **9**, 1955–1964 (2013).
71. J. D. Mintern *et al*., *Autophagy* **11**, 906–917 (2015).
72. D. Sancho *et al*., *Nature* **458**, 899–903 (2009).
73. S. Zelenay *et al*., *J. Clin. Invest.* **122**, 1615–1627 (2012).

ACKNOWLEDGMENTS

We thank the Alvin J. Siteman Cancer Center at Washington University School of Medicine for use of the Center for Biomedical Informatics and Multiplex Gene Analysis Genechip Core Facility; E. Tonc for blinded microscopy analysis; D. Oakley and J. Fitzpatrick for assistance with confocal microscopy, which was performed at Washington University Center for Cellular Imaging (WUCCI), supported by Washington University School of Medicine, the Children's Discovery Institute of Washington University and St. Louis Children's Hospital (CDI-CORE-2015-505), the Foundation for Barnes-Jewish Hospital (3770), and the National Institute for Diabetes and Digestive and Kidney Diseases (P30 DK020579); and R. Tomaino and the Taplin mass spectrometry core at Harvard University for performing mass spectrometry experiments. **Funding:** Supported by NIH grant T32 AI007163-40 (D.J.T.); NCI grants T32 CA 009621 (J.T.D.), 5R01 CA 190700 (R.D.S.), P30 CA 091842 (W.E.G.), and 5R01 CA 193318 (N.M.); NIAID grant U19-AI109948 (W.Y.); NIH grant F30DK108498 (V.D.); NSF grant DGE-1143954 (P.B.); NIH grant U19-AI109725 (H.W.V.); and the Howard Hughes Medical Institute (K.M.M.). WDFY4-deficient mice used in this study were generated by the JAX KOMP program (U42OD011185). **Author contributions:** D.J.T. and J.T.D. designed, performed, and analyzed most experiments; C.G.B. and P.B. performed and analyzed experiments; V.D., M.G., E.J.L., W.Y., Q.W., L.D.S., W.L.B., J.R.B., N.M., P.D., and M.S.D. designed, performed, and analyzed experiments; R.D.S. and H.W.V. generated models and designed experiments; and W.E.G., T.L.M., and K.M.M. designed experiments and wrote the manuscript. **Competing interests:** H.W.V. is a founder of Casma Therapeutics, Cambridge, MA. **Data and materials availability:** Microarray data have been deposited in the NCBI gene expression omnibus at accession number GSE118652; the mass spectrometry proteomics data have been deposited to the ProteomeXchange Consortium via the PRIDE partner repository with the data identifier PXD011210. All other data are available in manuscript or supplementary materials. WDFY4 knockout mice were obtained through the Knockout Mouse Project (KOMP) at the Jackson Laboratory (catalog number: 029334).

SUPPLEMENTARY MATERIALS

www.sciencemag.org/content/362/6415/694/suppl/DC1
Materials and Methods
Figs. S1 to S15
Tables S1 to S6
References (*74*–*85*)

5 March 2018; resubmitted 17 August 2018
Accepted 27 September 2018
10.1126/science.aat5030